

Original Article

Cite this article: Jiang Y, Yao D, Zhou J, Tan Y, Huang H, Wang MeiL, Chang X, Duan M, Luo C (2022). Characteristics of disrupted topological organization in white matter functional connectome in schizophrenia. *Psychological Medicine* **52**, 1333–1343. <https://doi.org/10.1017/S0033291720003141>

Received: 22 February 2020
Revised: 6 August 2020
Accepted: 12 August 2020
First published online: 3 September 2020


Key words:

Connectome; fMRI; graph theory; schizophrenia; white matter

Author for correspondence:

Cheng Luo,
E-mail: chengluo@uestc.edu.cn

Characteristics of disrupted topological organization in white matter functional connectome in schizophrenia

Yuchao Jiang^{1,2} , Dezhong Yao^{1,3,4}, Jingyu Zhou^{1,2}, Yue Tan¹, Huan Huang¹, MeiLin Wang¹, Xin Chang^{1,2}, Mingjun Duan^{1,5} and Cheng Luo^{1,2,3}

¹The Clinical Hospital of Chengdu Brain Science Institute, MOE Key Lab for Neuroinformation, Center for Information in Medicine, University of Electronic Science and Technology of China, Chengdu, P. R. China;

²High-Field Magnetic Resonance Brain Imaging Key Laboratory of Sichuan Province, School of life Science and technology, University of Electronic Science and Technology of China, Chengdu, P. R. China; ³Research Unit of NeuroInformation, Chinese Academy of Medical Sciences, 2019RU035, Chengdu, P. R. China; ⁴School of Electrical Engineering, Zhengzhou University, Zhengzhou, P. R. China and ⁵Department of Psychiatry, Chengdu Mental Health Center, Chengdu, P. R. China

Abstract

Background. Neuroimaging characteristics have demonstrated disrupted functional organization in schizophrenia (SZ), involving large-scale networks within grey matter (GM). However, previous studies have ignored the role of white matter (WM) in supporting brain function.

Methods. Using resting-state functional MRI and graph theoretical approaches, we investigated global topological disruptions of large-scale WM and GM networks in 93 SZ patients and 122 controls. Six global properties [clustering coefficient (C_p), shortest path length (L_p), local efficiency (E_{loc}), small-worldness (σ), hierarchy (β) and synchronization (S) and three nodal metrics [nodal degree (K_{nodal}), nodal efficiency (E_{nodal}) and nodal betweenness (B_{nodal})] were utilized to quantify the topological organization in both WM and GM networks.

Results. At the network level, both WM and GM networks exhibited reductions in E_{loc} , C_p and S in SZ. The SZ group showed reduced σ and β only for the WM network. Furthermore, the C_p , E_{loc} and S of the WM network were negatively correlated with negative symptoms in SZ. At the nodal level, the SZ showed nodal disturbances in the corpus callosum, optic radiation, posterior corona radiata and tempo-occipital WM tracts. For GM, the SZ manifested increased nodal centralities in frontoparietal regions and decreased nodal centralities in temporal regions.

Conclusions. These findings provide the first evidence for abnormal global topological properties in SZ from the perspective of a substantial whole brain, including GM and WM. Nodal centralities enhance GM areas, along with a reduction in adjacent WM, suggest that WM functional alterations may be compensated for adjacent GM impairments in SZ.

Introduction

Schizophrenia (SZ) is a severe psychiatric disorder that involves ineffective or inefficient communication between brain regions from neuroimaging evidence (Dong, Wang, Chang, Luo, & Yao, 2018). Although the pathological mechanism of SZ is unclear, the results of accumulated evidence have suggested widespread local abnormalities in several brain regions, including the insula (Moran et al., 2013), hippocampus (Ho et al., 2017), thalamus (Pergola, Selvaggi, Trizio, Bertolino, & Blasi, 2015; Wang et al., 2020), striatum (Duan et al., 2015; McCutcheon, Abi-Dargham, & Howes, 2019), frontal lobes (Chen et al., 2017a), temporal regions (Jiang et al., 2018) and cerebellum (Dong et al., 2020). Previous studies have also reported that some neural circuits or pathways, such as the prefrontal-thalamic-cerebellar pathway (Gong et al., 2019; Guo et al., 2015; Jiang et al., 2019a) and the triple network circuit of the salience, default mode and central executive networks (Dong et al., 2018; Menon, 2011), play important roles in the pathophysiology of SZ. These findings suggest that this disease is associated with global topological disruptions of large-scale brain networks in patients with SZ.

In general, large-scale brain networks can be summarized into structural networks (anatomical connectivity) and functional networks (temporal synchronization) (Bullmore & Sporns, 2009). Using diffusion tensor imaging (DTI), anatomical connections (i.e. fibre tracts) between distinct brain regions can be estimated to build a structural network, which uncovers the structural architecture in brain white matter (WM). However, it fails to provide temporal dynamic information, which may carry functional significance in WM. Based on the blood oxygen level-dependent (BOLD)-functional magnetic resonance imaging (fMRI), the

functional network is usually calculated by temporal correlations between BOLD-fMRI signals among distributed brain regions, which is thought to reflect neural activity or relevant functions that occur in grey matter (GM). Investigations on the WM structural network or GM functional network have ignored the presence of potential functional information in WM, although they provide precise details concerning brain network architecture.

In recent years, increasingly more works have indicated that brain functional activation in WM can be detected by using BOLD-fMRI. For instance, specific regions of the corpus callosum were shown to be functionally activated in multiple tasks, such as interhemispheric transfer tasks (Courtemanche, Sparrey, Song, MacKay, & D'Arcy, 2018; Gawryluk, Mazerolle, Beyea, & D'Arcy, 2014a). Low-frequency BOLD fluctuations in specific WM tracts can be modulated by different behaviour tasks (Huang *et al.*, 2018; Marussich, Lu, Wen, & Liu, 2017; Wu *et al.*, 2017). In particular, recent work demonstrated that compared with cortical GM, WM tracts exhibited reduced magnitudes, delayed onsets and prolonged initial dips in haemodynamic response function (Li, Newton, Anderson, Ding, & Gore, 2019b). More than task-state fMRI, resting-state BOLD-fMRI signals within WM showed an intrinsic functional organization rather than random noise, similar to GM functional networks (Jiang *et al.*, 2019b; Peer, Nitzan, Bick, Levin, & Arzyt, 2017). Moreover, specific WM tracts, identified from BOLD-fMRI signals, showed a similar pattern with the fibre bundles from DTI tracking in the human brain (Marussich *et al.*, 2017; Peer *et al.*, 2017). Furthermore, histological evidence reconfirmed the similarities between functional connectivity and anatomical connectivity in non-human primate brains (Wu *et al.*, 2019). In addition to healthy brains, WM functional connectivity has been reported to be altered in abnormal brains, including in individuals with mild cognitive impairment, epilepsy, schizophrenia, Alzheimer's disease and Parkinson's disease (Chen *et al.*, 2017b; Ji *et al.*, 2019; Jiang *et al.*, 2019c; Makedonov, Chen, Masellis, MacIntosh, & Alzheimer's Disease Neuroimaging, 2016). This evidence from multi-state (tasks and resting-state) and multimodal MRI (BOLD-fMRI and DTI) findings in multiple brain types (healthy, abnormal and non-human brains) converges to support WM functional information revealed by BOLD-fMRI.

While previous studies investigated functional interactions among specific WM tracts, we wanted to further examine the features of the functional connectome of large-scale networks in WM, which could reflect some differences in brain network architectures or mechanisms. Graph theoretical analysis is an effective approach to characterize topological features of brain networks (Bullmore & Sporns, 2009). Findings revealed after applying graph theory to GM functional networks have suggested that GM functional networks are organized to allow optimized efficiency, such as that observed in small-worldness (Bullmore & Sporns, 2009). Combined with graph-theoretical analyses, a large-scale WM functional network has promised a new way to characterize the topological properties of functional networks in WM and has improved our understanding of WM dysfunctions that underlie the clinical symptoms of SZ. In addition, while previous studies used resting-state fMRI and graph theory approaches to investigate the topological organization of the functional connectome in patients with SZ (Yu *et al.*, 2017), they ignored WM functional information that was potentially available. Here, to extend our understanding of schizophrenia from the topological organization of brain WM network architectures, we investigated the resting-state large-scale WM functional

network in a large cohort of patients with SZ ($n = 97$) and healthy subjects ($n = 126$). Graph theoretical analysis was utilized to quantify the topological organization in the WM functional network. By comparing the differences in topological properties between patients and controls, we explored the disorganisation of the WM functional connectome within schizophrenia pathophysiology.

Methods

Subjects and MRI acquisition

In total, 97 patients with SZ (29 females; age: 41.0 ± 11.5 years) and 126 healthy subjects (HC) (42 females; age: 38.0 ± 14.9 years) who matched in age, gender and education were recruited from the Clinical Hospital of Chengdu Brain Science Institute (CHCBSI) of China. All of the SZ patients were diagnosed according to the Diagnostic and Statistical Manual of Mental Disorder, Fourth Edition (DSM-IV). Of the 97 SZ patients, two were first-episode patients and 95 were chronic patients. All patients received antipsychotics medication [Chlorpromazine (CPZ) equivalents = 324.5 ± 157.1 mg/day]. Clinical symptoms were evaluated by the Positive and Negative Syndrome Scale (PANSS). Participants with a history of major medical or neurological abnormalities, substance abuse, or other contraindications to MRI were excluded from the current study. To further eliminate the potential familial effects, we also excluded the healthy subjects whose first- and second-degree relatives have a history with mental disorders. Written informed consent was signed from each participant before the MRI scanning. The Ethics Committee of CHCBSI approved this current study.

High-resolution T1-weighted images, resting-state fMRI and diffusion-weighted images were acquired in a 3.0 Tesla GE MRI scanner (DISCOVERY MR 750, USA) at the Centre for Information in Medicine of University of Electronic Science and Technology of China. Details of scanning parameters were obtained from our previous studies (Jiang *et al.*, 2019b).

Diffusion data processing

Diffusion images were analysed using the tract-based spatial statistics (TBSS) method in the FSL software (<https://www.fmrib.ox.ac.uk/fsl>). First, eddy current distortions and head motion correction, as well as brain extraction, were performed. For each subject, the fractional anisotropy (FA) map was estimated by fitting the diffusion tensor model. All subjects' FA maps were non-linearly transformed into the MNI template. Subsequently, the averaged FA map across all subjects was thinned to create a FA skeleton image, which represented the major WM tracts common to the group. Finally, individual FA image was projected into the FA skeleton.

Functional image pre-processing

Functional images processing was performed using the SPM12 (<http://www.fil.ion.ucl.ac.uk/spm/software/spm12>), DPABI (<http://www.restfmri.net>) and FSL software. Image preprocessing was similar to our previous studies (Jiang *et al.*, 2019b). The first five volumes were removed. Slice timing correction and realignment was performed. Subjects with maximum motion >2 mm or 2° were excluded. The mean frame displacement (FD) was also calculated for each subject. Subsequently, a linear trend was removed for the

signal drift correction. Nuisance signals, including the 24-parameter head motion, the mean CSF signal and scrubbing time points (FD > 0.5 mm), were further regressed out by a multiple linear model. Then, the band-pass filtering (0.01–0.10 Hz) was performed to reduce potential physiological signals. Spatial smoothing (FWHM = 4 mm) was performed separately within the white matter or grey matter masks, which were obtained from the individual T1 images segmentation. Finally, functional images were normalized onto the MNI space and resampled into 3 mm³. It's important to be clear that the WM network construction was performed on the unsmoothed pre-normalized functional data. In addition, data quality control pipeline is also described in the online Supplementary Material.

Large-scale functional network in GM and WM

According to the Harvard-Oxford atlas (Desikan et al., 2006), the cortical grey matter was divided into 96 regions of interest (ROIs). The averaged time series of each ROI was extracted from the normalized functional images for each subject. Then, Pearson's correlation coefficient was calculated between any two paired ROIs and further transformed to Fisher's z score. This resulted in a 96 × 96 correlation matrix for the GM of each participant.

For the WM, the JHU WM atlas was used to yield 48 tracts (21 tracts in each hemisphere and six commissure tracts). For each subject, the pre-normalization unsmoothed functional images were filtered (0.01–0.15 Hz) (Jiang et al., 2019b; Peer et al., 2017), then registered to the corresponding diffusion b0 image and then nonlinearly projected onto the FA skeleton using the transformation function from the TBSS analysis. This resulted in a series of skeletonized functional images. The averaged time series of each WM tract was extracted from the skeletonized functional images. A 48 × 48 correlation matrix for the WM was also produced using Pearson's correlation between each paired WM tract for each subject.

Network properties

We used GREYNA (<http://www.nitrc.org/projects/gretna/>) to analyse the network properties using graph theory.

First, each correlation matrix was further transformed into an undirected binarized matrix using a sparsity threshold. The sparsity of a network was computed as the ratio of the existing number of edges divided by the maximum possible number of edges for a given network. According to previous research (Yu et al., 2017), we used a wide range of sparsity thresholds to binarize the correlation matrix. The range of the sparsity threshold was defined as follows: (1) the averaged degree (the degree of a node is the number of connections linked to the node) over all nodes of each binarized network was larger than $2 \times \log(N)$, where N is the number of nodes; and (2) the small-worldness of the binarized networks was larger than 1.1 for 90% of the subjects. A range of sparsity thresholds (WM network: 0.19–0.52, GM functional network: 0.11–0.46) could be preselected. To achieve a unified standard, we finally chose an overlapping range (0.19–0.46, with a step of 0.01) between the WM and GM networks.

Second, to characterize the topological properties of WM and GM networks, six global network parameters, including the clustering coefficient (C_p), shortest path length (L_p), local efficiency (E_{loc}), small-worldness metric (σ), hierarchy (β) and synchronization (S), were calculated for the WM and GM network at each sparsity threshold. According to previous studies (Barahona &

Pecora, 2002), network synchronization is quantified by the eigenratio of the Laplacian matrix (coupling matrix) of the network. The lower eigenratio represents a more easily synchronized network. In addition, three nodal metrics, including the nodal degree (K_{nodal}), nodal efficiency (E_{nodal}) and nodal betweenness (B_{nodal}), were utilized for regional topological measures. The rationale for each graphic parameter is listed in the online Supplementary Materials. The uses and interpretations of these complex network properties have been described in previous research (Chen, Hu, Chen, & Feng, 2019; Rubinov & Sporns, 2010).

Third, to validate the nonrandomness of topological properties, WM and GM networks were compared to random networks. In line with previous studies, the generation of random networks was accomplished using a Markov chain algorithm, which could yield the same number of nodes, edges and degree of distribution as the matched actual brain networks. Furthermore, the z-score of each network parameter was calculated by subtracting the average of each parameter across random networks and then dividing it by the standard deviation of random networks.

Finally, the area under the curve (AUC) for each network parameter was calculated to yield a summarized scalar for the topological characterization of brain networks independent of a single threshold selection.

Statistical analysis

To investigate the differences of network topological properties between the SZ and HC groups, nonparametric permutation tests were performed. In brief, for each network parameter, we calculated the real difference value between the two groups. Then, we randomly assigned the group labels across all subjects and recalculated the difference value between the two randomized groups. This randomization procedure was repeated 100 000 times and thus yielded a distribution of the null hypothesis. According to the location of the real difference value within the distribution of the null hypothesis, a p value was assigned to the real difference. Statistical significance was assessed by the 95th percentiles of each distribution of the null hypothesis, corresponding to a type I error probability of 0.05 for a two-tailed test.

To further examine the associations between the altered nodal metrics (K_{nodal} , E_{nodal} and B_{nodal}) and FA values, the WM tracts with altered nodal metrics were extracted and then Spearman rank correlation analysis was used to evaluate the correlation between the nodal metrics and FA for altered WM tracts in each group. Non-parametric permutation tests were performed to test the group interaction that whether the difference in correlations between SZ and HC groups is significant (online Supplementary Materials).

For the abnormal network metrics in the SZ group, we further explored the relationships between these metrics and PANSS symptom scores as well as illness duration by using Spearman rank correlation analysis.

Results

Demographic and clinical characteristics

Four SZ patients and four HC were excluded because they failed to accomplish all of T1, resting-state fMRI and DTI data acquisitions, or their head-motion beyond 2 mm or 2°. The remaining 93 patients with SZ (28 females; age: 40.01 ± 11.49 years) and

Table 1. Demographic and clinical characteristics of subjects

Characteristic	SZ Mean (s.d.)	HC Mean (s.d.)	<i>p</i> value
Number ^a	93	122	
Gender (M/F)	28/65	41/81	0.586 ^b
Age (years)	40.01 (11.49)	37.95 (14.74)	0.267 ^c
Education (years)	11.47 (2.51)	11.07 (3.22)	0.299 ^c
Illness duration (years)	15.22 (10.27)	–	–
Chlorpromazine equivalents (mg/day)	337.96 (145.26)	–	–
PANSS score			
Total	62.21 (13.26)	–	–
Positive	13.32 (5.89)	–	–
Negative	20.70 (6.06)	–	–
General	28.19 (5.86)	–	–

^aRepresents that four SZ patients and four HC were excluded from original database (97 SZ and 126 HC) because they failed to accomplish all of the T1, resting-state fMRI and DTI data acquisitions, or their head-motion beyond 2 mm or 2°.

^b*p* value was obtained by the χ^2 test.

^c*p* value was obtained using the two-sample *t* test.

122 HC (41 females; age: 37.95 ± 14.74 years) were matched in age ($p = 0.267$), gender ($p = 0.586$) and education ($p = 0.299$). Demographic and clinical characteristics of these subjects is provided in Table 1.

Global topological properties of functional brain networks in schizophrenia

For both the WM and GM networks, the small-worldness scalars in the two groups were larger than 1 at a sparsity threshold range of 0.19–0.46; i.e. the functional networks exhibited higher clustering coefficients, such as those associated with regular lattices, yet small shortest path lengths, such as those associated with random graphs. This indicated that both the WM and GM functional connectomes exhibited typical small-worldness topology.

Between-group comparisons on the AUC of network properties showed that compared with the HC group, patients with SZ showed significantly lower values in E_{loc} ($p = 0.021$), L_p ($p = 0.019$), C_p ($p = 0.031$) and synchronization ($p = 0.003$) for the GM functional network (Fig. 1a). No significant differences were observed in small-worldness ($p = 0.248$) and hierarchy ($p = 0.424$).

For the WM functional connectome, the SZ group exhibited significant reductions in E_{loc} ($p = 0.028$), C_p ($p = 0.047$), small-worldness ($p = 0.025$), hierarchy ($p = 0.009$) and synchronization ($p = 0.042$) compared with the HC group (Fig. 1b). There was no significant difference in L_p ($p = 0.286$).

These group differences were further validated through an additional stability analysis (online Supplementary Material).

Regional topological organization in schizophrenia

We further identified the cortical GM regions or WM tracts exhibiting significant group differences in nodal metrics (K_{nodal} , E_{nodal} and B_{nodal}) in patients with SZ. K_{nodal} and E_{nodal} values showed a

similar alteration pattern in the patient group (Fig. 2). No significant group difference was identified for the B_{nodal} values.

For cortical GM, regions showing significant group differences in K_{nodal} or E_{nodal} values were localized primarily in the frontal, parietal and temporal lobes (Fig. 2a and Table 2). Specifically, in comparison with the HC group, the SZ group showed increased K_{nodal} or E_{nodal} values in the bilateral frontal lobes (superior frontal gyrus and middle frontal gyrus), bilateral parietal lobes (angular gyrus, posterior supramarginal gyrus and precuneus cortex), bilateral occipital lobes (superior lateral occipital cortex) and limbic regions (posterior cingulate gyrus) ($p < 0.05$, Bonferroni corrected) (Fig. 2a and Table 2). Additionally, lower K_{nodal} or E_{nodal} values were found in most of the temporal lobes (temporal pole, superior temporal gyrus, middle temporal gyrus, parahippocampal gyrus, temporal fusiform cortex, planum polare, Heschl's gyrus and planum temporale), subcallosal cortex, parietal operculum cortex and left central opercular cortex ($p < 0.05$, Bonferroni corrected) (Fig. 2a and Table 2).

For the WM tracts, the patients with SZ exhibited increased nodal topology (K_{nodal} or E_{nodal}) in the following brain regions: the body of the corpus callosum, left medial lemniscus, left superior cerebellar peduncle, right posterior limb of internal capsule and right external capsule ($p < 0.05$, Bonferroni corrected) (Fig. 2b and Table 3). Regions showing reduced nodal topology were found in the splenium of the corpus callosum, left anterior corona radiata, bilateral posterior corona radiata, bilateral optic radiation, left sagittal stratum and bilateral tapetum ($p < 0.05$, Bonferroni corrected) (Fig. 2b and Table 3). These group differences were further validated through an additional stability analysis (online Supplementary Material).

We also found correlations between the E_{nodal} and FA values in the right posterior limb of the internal capsule ($r = -0.234$, $p = 0.010$, FDR corrected), left ($r = -0.180$, $p = 0.048$, uncorrected) and right optic radiation ($r = -0.199$, $p = 0.029$, uncorrected) in the HC group (Fig. 2c). However, these correlations were not significant in the SZ group (all $p > 0.05$). Furthermore, these correlations between the E_{nodal} and FA values in the right posterior limb of the internal capsule ($p = 0.001$, Bonferroni corrected) and right optic radiation ($p = 0.008$, Bonferroni corrected) showed significant differences between two groups using nonparametric permutation tests.

Relationships between network measures and clinical variables

After multiple comparisons correction by the false discovery rate ($p < 0.05$, FDR corrected), the lower C_p ($r = -0.275$, $p = 0.010$), L_p ($r = -0.260$, $p = 0.016$) and E_{loc} ($r = -0.288$, $p = 0.007$) of the GM network showed significantly negative correlations with illness duration in the SZ group (Fig. 3a). In addition, the lower C_p ($r = -0.294$, $p = 0.019$), E_{loc} ($r = -0.301$, $p = 0.017$) and synchronization ($r = -0.311$, $p = 0.013$) of the GM network exhibited significant negative correlations with the PANSS negative scores (Fig. 3b). For WM, there was no significant correlation between network properties and clinical variables after FDR multiple comparisons correction.

Discussion

Using The graph theory approach, this study presented a novel network perspective for investigating how the resting-state WM and GM function altered for SZ patients in a comprehensive set

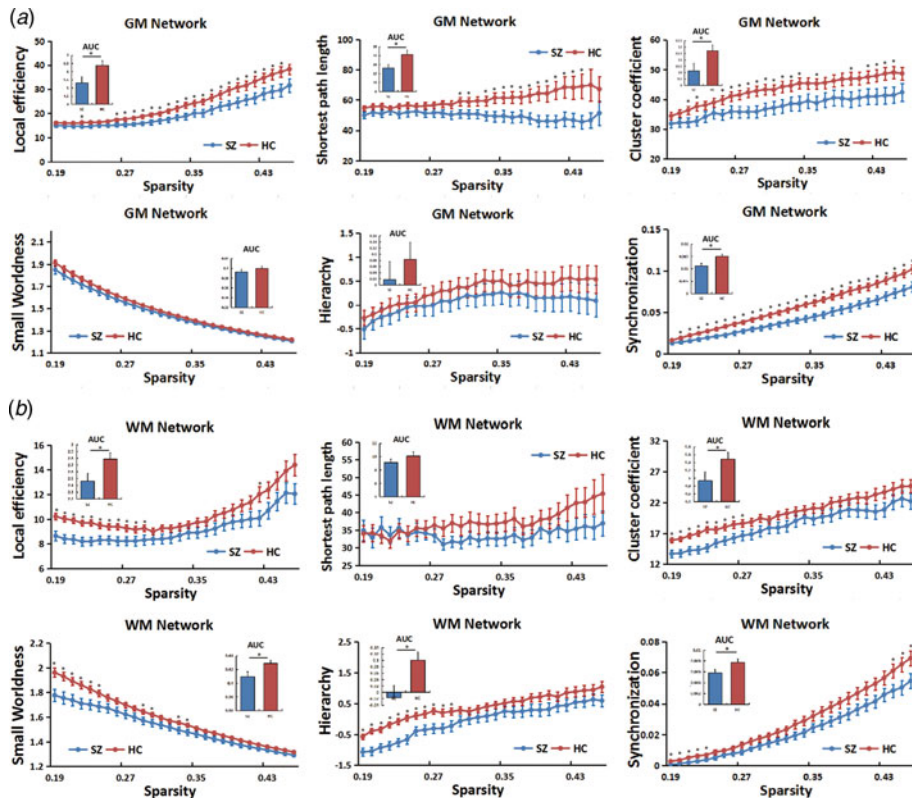


Fig. 1. Group differences in the topological properties of functional (a) grey matter and (b) white matter networks between the schizophrenia patients and healthy controls. In the grey matter network, the area under curve of local efficiency ($p = 0.021$), shortest path length ($p = 0.019$), cluster coefficient ($p = 0.031$) and synchronization ($p = 0.003$) were significantly lower in the schizophrenia group compared to the healthy control group (according to the nonparametric permutation test). No significant differences were observed in small worldness ($p = 0.248$) and the hierarchy ($p = 0.424$) between the two groups. In the white matter network, the area under curve of local efficiency ($p = 0.028$), cluster coefficient ($p = 0.047$), small worldness ($p = 0.025$), hierarchy ($p = 0.009$) and synchronization ($p = 0.042$) were significantly lower in the schizophrenia (SZ) group compared to the healthy control (HC) group (according to the nonparametric permutation test). No significant differences were identified in the shortest path length ($p = 0.286$) between the two groups. Note: GM, grey matter; WM, white matter; SZ, schizophrenia; HC, healthy controls; AUC, area under curve.

at both global and nodal levels. At the global level, both the WM and GM networks exhibited reductions in the local efficiency, cluster coefficient and synchronization in the SZ group relative to the values observed for the controls. In addition, patients with SZ showed reduced small-worldness and hierarchy only for the WM network. Furthermore, the cluster coefficient, local efficiency and synchronization of the WM network were significantly negatively correlated with the PANSS negative score in patients with SZ. At the nodal level, the SZ group showed specific WM nodal disturbances in the corpus callosum, optic radiation, posterior corona radiata and tempo-occipital WM tracts. Regarding GM, the SZ group manifested increased nodal topology in fronto-parietal regions and decreased nodal topology in temporal regions. These findings advance our understanding of disrupted WM function underlying the pathological mechanism of SZ from a functional topology perspective.

Abnormalities in functional segregation (E_{loc} and C_p) and functional integration (L_p) are key features of brain network disorganization in SZ. E_{loc} represents the efficiency of information exchange within a local subnetwork or among adjacent regions, while C_p measures the degree of nodes tending to cluster together (Rubinov & Sporns, 2010). This study observed that both GM and WM functional networks showed reduced E_{loc} and C_p in SZ, which was compatible with prior studies reporting lower local information transfer in SZ (Fornito, Zalesky, Pantelis, & Bullmore, 2012). These findings further supported that decreased functional segregation might be a common feature of brain network disorganization in SZ, regardless of GM and WM. Reduced efficiency in local communication (i.e. functional segregation) of brain networks may arise from neurodevelopmental impairments, which were demonstrated not only in cortical GM (including excessive synaptic elimination) (Sellgren et al., 2019),

but also by abnormal WM neurobiology (including impaired WM integrity) (Kochunov & Hong, 2014) in SZ. As one of the metrics in functional integration, L_p measures the shortest distance from one node to other nodes in a network (Rubinov & Sporns, 2010). The lower L_p reveals enhanced functional integration for information transfer in the brain network. Consistent with previous studies (Yu et al., 2017), patients with SZ also exhibited increased functional integration in the large-scale GM functional network. It is thought that the enhanced functional integration in SZ indicates greater resilience to focal neural damage in GM (Lo et al., 2015; Lynall et al., 2010). In neuroimaging studies, focal damage could be referred to as ‘lesions’ of GM and WM, and included observations such as reduced GM volume, thinner cortical thickness or impaired myelination measured by diffusion MRI. Brain network topological resilience has been assumed to protect the integrity of the network from pathological attack in SZ (Lo et al., 2015). However, in the current study, greater functional integration in SZ was only observed in GM, not in the WM network, which indicated that WM did not present greater resilience to focal damage. We hypothesized that within WM, abnormal functional information from focal damage is more likely to spread to other WM areas along the fibre tracts. Furthermore, the present study found negative correlations between the E_{loc} , C_p and PANSS negative scores, indicating that the brain topological network was associated with the severity of illness. This result implied that the brain topological network may predict SZ clinical symptoms. These brain network features were also correlated with illness duration, which provided evidence that progressive abnormalities of the brain topological network occurred in SZ.

Synchronization plays a crucial role in precise information processing of the brain (Fries, 2009). Accumulated evidence

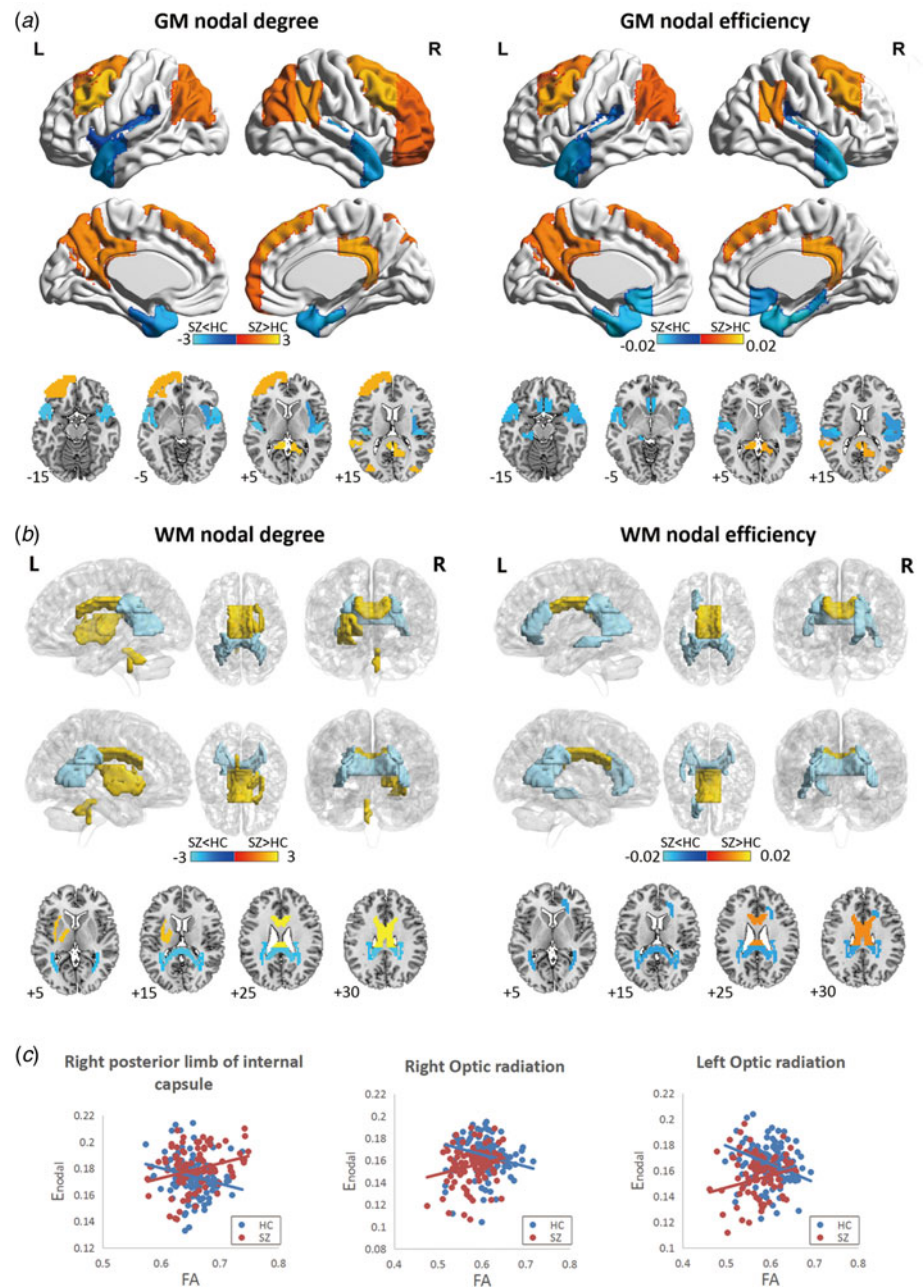


Fig. 2. Cortical grey matter regions (a) and white matter tracts (b) exhibiting abnormal nodal degree and nodal efficiency in patients with schizophrenia by using the nonparametric permutation test ($p < 0.05$, Bonferroni corrected). The colour bar indicates the between-group difference values; the yellow regions represent higher and blue regions represent lower nodal degree or nodal efficiency in the patient group compared with the control group. (c) Significant correlations between the E_{nodal} and the FA values in the right posterior limb of internal capsule, left and right optic radiation in the HC group. *Note:* GM, grey matter; WM, white matter; SZ, schizophrenia; HC, healthy controls; L, left; R, right; FA, fractional anisotropy.

from EEG, MEG and fMRI studies has suggested that SZ is related to impaired neural synchrony (Ford, Krystal, & Mathalon, 2007; Uhlhaas & Singer, 2010). These synchrony disruptions have been also demonstrated to be associated with the core cognitive impairments and symptom severity, suggesting abnormal neurobiological processes in SZ (Uhlhaas, Haenschel, Nikolic, & Singer, 2008). However, most studies evaluated brain synchronization using the temporal correlation in local oscillations or the functional connectivity of distributed brain regions, rather than whole-brain network features. The eigenratio of the graph Laplacian matrix is believed to be a frequently used indicator of synchronizability in complex networks (Barahona & Pecora, 2002). Using this approach, the present study found that both WM and GM functional networks of SZ patients exhibited excessive synchronizability (i.e. decreased eigenratio). Moreover, the altered synchronization of the WM network was associated with

more severe negative symptoms in SZ. These findings provide evidence of disrupted brain network synchronizability in SZ.

In addition, abnormalities of hierarchy and small-worldness of brain networks have been widely reported in substantial neuroimaging studies, although the alterations were not always consistent in SZ. For example, Bassett *et al.* (2008) reported less hierarchy in a sample of 203 people with SZ, while Lynall *et al.* (2010) found enhanced hierarchy in patients with SZ compared to that in healthy volunteers. Additionally, several studies found that people with SZ showed reduced small-worldness (Liu *et al.*, 2008); however, some studies observed that there were no significant differences in small-worldness between patients and controls (Yu *et al.*, 2017). In the current study, patients with SZ showed reduced hierarchy and small-worldness only in the WM functional network but not in the GM network. One possible explanation is that the possible physiological base of BOLD signals in the

Table 2. Cortical grey matter regions that exhibited altered nodal topological organization in patients with schizophrenia v. healthy control subjects

Region	Nodal betweenness		Nodal degree		Nodal efficiency	
	Difference	<i>p</i> values	Difference	<i>p</i> values	Difference	<i>p</i> values
Frontal regions						
Left Superior frontal gyrus	1.18	0.3290	1.74	<0.0001*	0.010	0.0002*
Right Superior frontal gyrus	0.98	0.5314	1.94	<0.0001*	0.012	0.0001*
Left Middle frontal gyrus	2.66	0.0103	2.33	<0.0001*	0.014	<0.0001*
Right Middle frontal gyrus	1.92	0.0440	2.26	<0.0001*	0.014	<0.0001*
Left Subcallosal cortex	0.70	0.3287	-1.09	0.0039	-0.016	0.0002*
Right Subcallosal cortex	1.40	0.1907	-0.93	0.0181	-0.013	0.0004*
Temporal regions						
Left Temporal pole	-0.64	0.8224	-2.08	0.0005*	-0.015	0.0004*
Right Temporal pole	-0.56	0.8072	-2.15	<0.0001*	-0.017	0.0001*
Left Superior temporal gyrus, anterior division	-0.75	0.6333	-1.67	0.0002*	-0.013	<0.0001*
Right Superior temporal gyrus, anterior division	-0.09	0.9618	-2.03	<0.0001*	-0.015	<0.0001*
Left Middle temporal gyrus, anterior division	-1.78	0.1497	-1.27	0.0023	-0.012	0.0002*
Right Middle temporal gyrus, anterior division	-2.74	0.0343	-1.48	0.0009	-0.014	<0.0001*
Left Parahippocampal gyrus, anterior division	-2.02	0.0977	-1.72	0.0003*	-0.017	0.0001*
Right Parahippocampal gyrus, anterior division	-4.95	0.0016	-2.33	<0.0001*	-0.019	<0.0001*
Right Parahippocampal gyrus, posterior division	-2.49	0.0172	-1.36	0.0007	-0.015	0.0001*
Left Temporal fusiform cortex, anterior division	-2.25	0.0226	-1.69	0.0001*	-0.018	<0.0001*
Left Planum polare	-0.97	0.3287	-1.78	<0.0001*	-0.016	<0.0001*
Right Planum polare	-0.91	0.2968	-1.84	<0.0001*	-0.015	0.0001*
Left Heschls gyrus	-2.13	0.0086	-1.90	<0.0001*	-0.015	<0.0001*
Right Heschls gyrus	-1.88	0.0406	-2.18	<0.0001*	-0.017	<0.0001*
Left Planum temporale	-1.22	0.3539	-1.17	0.0026	-0.009	0.0002*
Right Planum temporale	-0.69	0.5211	-1.33	0.0005	-0.010	<0.0001*
Parietal regions						
Left Angular gyrus	1.16	0.2526	1.46	<0.0001*	0.009	0.0001*
Right Angular gyrus	1.18	0.0965	1.89	<0.0001*	0.013	<0.0001*
Right Supramarginal gyrus, posterior division	0.95	0.3389	1.82	<0.0001*	0.011	<0.0001*
Left Precuneus cortex	0.92	0.3257	1.68	0.0001*	0.010	0.0001*
Left Parietal operculum cortex	-1.53	0.1329	-1.36	0.0001*	-0.010	<0.0001*
Right Parietal operculum cortex	-0.93	0.3339	-1.21	0.0011	-0.009	0.0001*
Occipital regions						
Left Lateral occipital cortex, superior division	-0.72	0.6529	1.49	0.0002*	0.008	0.0003*
Right Lateral occipital cortex, superior division	-0.24	0.8714	1.42	0.0005*	0.008	0.0012
Limbic regions						
Left Cingulate gyrus, posterior division	2.24	0.0583	1.74	<0.0001*	0.011	0.0003*
Right Cingulate gyrus, posterior division	2.15	0.0103	2.05	<0.0001*	0.013	<0.0001*
Frontoparietal junction						
Left Central opercular cortex	-0.97	0.4044	-1.20	0.0013	-0.009	0.0003*

Note: * represents $p < 0.05$, Bonferroni correction.

Table 3. White matter tracts that exhibited altered nodal topological organization in patients with schizophrenia v. healthy control subjects

Region	Nodal betweenness		Nodal degree		Nodal efficiency	
	Difference	<i>p</i> values	Difference	<i>p</i> values	Difference	<i>p</i> values
Body of corpus callosum	2.32	0.0349	0.92	0.0001*	0.013	0.0001*
Splenium of corpus callosum	1.07	0.4783	-0.73	0.0002*	-0.011	0.0001*
Left Medial lemniscus	-0.20	0.7150	0.61	0.0007*	0.006	0.1704
Left Superior cerebellar peduncle	1.42	0.1607	0.72	0.0002*	0.012	0.0016
Right Posterior limb of internal capsule	2.62	0.0155	0.60	0.0002*	0.005	0.0280
Left Anterior corona radiata	-0.84	0.3276	-0.55	0.0100	-0.011	0.0008*
Right Posterior corona radiata	1.02	0.0664	-0.56	0.0001*	-0.011	0.0001*
Left Posterior corona radiata	0.52	0.4218	-0.65	0.0001*	-0.011	0.0002*
Right Optic radiation	1.44	0.0148	-0.61	0.0001*	-0.012	<0.0001*
Left Optic radiation	1.23	0.0637	-0.58	0.0003*	-0.011	0.0001*
Left Sagittal stratum	-2.10	0.0448	-0.72	0.0011	-0.012	0.0005*
Right External capsule	0.04	0.9656	0.58	0.0004*	0.006	0.0087
Right Tapetum	-0.29	0.3052	-0.93	<0.0001*	-0.020	<0.0001*
Left Tapetum	-0.05	0.5965	-0.59	0.0004*	-0.015	0.0001*

Note: * represents $p < 0.05$, Bonferroni correction.

WM network is different from that in GM. In GM, postsynaptic potentials give rise to BOLD signals, whereas the precise source of BOLD signals in WM is complex. Previous studies put forward two possible interpretations for WM BOLD signals: spiking-related metabolic demands (Smith et al., 2002) and the activity of astrocytes and NO-producing neurons (Barbarelli, Fabri, & Mensa, 2014; Petzold & Murthy, 2011). This may suggest that the WM network may carry specific functional information that is different from the GM. Compared to the GM functional network, the WM functional network showed lower small-worldness, suggesting weaker segregation and a preference for global integration (Li et al., 2019a). WM tracts exhibited reduced magnitudes, delayed onsets and prolonged initial dips in haemodynamic response function compared with cortical GM (Li et al., 2019b). Additionally, WM functional networks were found to be organized in three layers (superficial, middle and deep), suggesting a possible hierarchical organization in information transfer within WM (Peer et al., 2017). Furthermore, recent studies have also found that the functional interactions among the three layers of WM networks were disrupted in SZ (Fan et al., 2020). Taken together, these findings were compatible with previous studies reporting less hierarchy and less small-worldness in patients with SZ, which might be expected to disrupt demands in higher-order cognitive processing.

At the nodal level, abnormalities in nodal attributes of GM, involving frontal, parietal, temporal, occipital and limbic regions, were found in the SZ group. These GM regions have been widely reported to show disrupted functional activations and structural deficits in SZ patients (Jiang et al., 2018; Luo et al., 2019). Moreover, abnormalities in these GM regions have also been reported to be associated with impairments of high-order cognitive function in SZ (Menon, 2011). In addition to the altered GM regions, specific WM regions involving the corpus callosum, posterior corona radiata, optic radiation and tempo-occipital WM tracts exhibited aberrant nodal centralities in SZ patients. Disrupted WM integrity in these regions has been previously

demonstrated in first-episode and chronic patients (Aydin, Uçok, & Guler, 2008; Bora et al., 2011) and has been associated with disease duration, symptom severity and cognitive functions (Rosenberger et al., 2012; Whitford et al., 2010). As an interhemispheric WM tract, the corpus callosum plays an essential role in maintaining stable information transfer between hemispheres (Shen et al., 2015). The abnormalities of the corpus callosum may disrupt interhemispheric functional communication in SZ (Agcaoglu et al., 2018; Wang et al., 2019). Several WM functional studies have also shown altered low-frequency oscillation amplitudes and functional connectivity in the corpus callosum for SZ patients (Jiang et al., 2019b; Yang et al., 2019). Consistent with these findings, the current results implied that the corpus callosum may play a notable role in maintaining stable functional interactions in the WM network, which was disrupted in SZ patients. Furthermore, prior studies suggested that WM functional changes may also be associated with GM function in SZ patients (Jiang et al., 2019b; Yang et al., 2019). Interestingly, this study observed abnormal functional increases in parietal and occipital GM areas in SZ, and these GM regions were connected to the posterior corona radiata and splenium of the corpus callosum. However, the posterior corona radiata and splenium of the corpus callosum exhibited functional decreases in SZ patients, which suggested that WM functional alterations may play a possible compensatory role for the adjacent GM impairments in SZ. Although non-invasive transcranial magnetic stimulation (TMS) has shown potential as a treatment for SZ, its mechanism remains unclear. Most TMS equipment can effectively act on the superficial cortical region. It has been hypothesized that TMS effects could reach distant areas via WM fibre tracts; thus, investigating the WM functional network may improve the present understanding of the mechanism of TMS in SZ treatment. In general, these abnormalities in WM extended the understanding of the pathophysiology of SZ from the perspective of the WM functional network.

The relationship between structure and function in WM is still inconclusive. Several studies have reported a significant

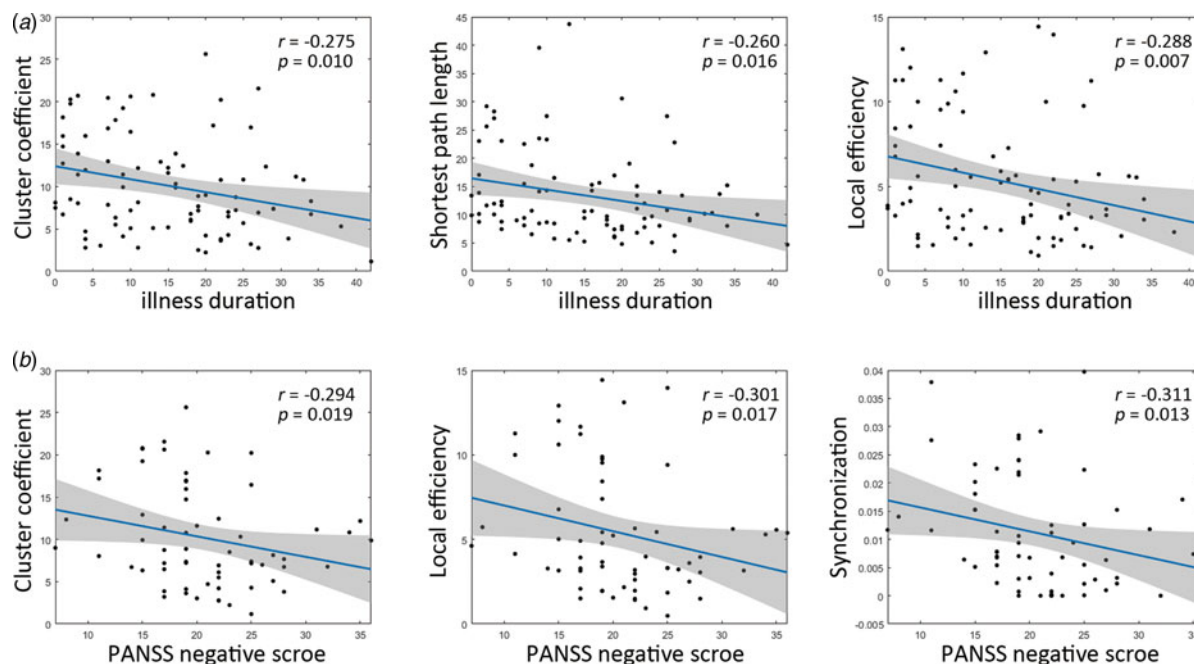


Fig. 3. The relationships between network metrics and clinical variables in patients with schizophrenia by using Spearman rank correlation analysis ($p < 0.05$, false discovery rate corrected). (a) The cluster coefficient, shortest path length and local efficiency were significantly negatively correlated with the illness duration. (b) The cluster coefficient, local efficiency and synchronization exhibited significant negative correlations with the PANSS negative scores.

correlation between WM activation and the FA value (Ji, Liao, Chen, Zhang, & Wang, 2017; Ji et al., 2019), whereas Yang's study showed no relationship of this structure and function in WM (Yang et al., 2019). Additionally, previous studies have suggested that the functional features detected by BOLD-fMRI can be partly explained by structural properties (Ji et al., 2017; Wu et al., 2019). We also found a negative correlation between the E_{nodal} and FA values at the posterior limb of the internal capsule and optic radiation in HCs. FA reflects the axonal density and myelination degree (Beaulieu, 2002). In WM, axons act as the pathway for information transfer. The transfer speed is improved by the myelin sheath produced by oligodendrocytes. In addition to oligodendrocytes, microglia and astrocytes are also present in WM. They provide nutrients and oxygen to neurons. In addition, astrocytes, which mediate neurovascular coupling in GM, are also found in WM (Rash, 2010). Taken together, these findings provide extended evidence on the association of structure and function in WM, suggesting a structural basis for BOLD-fMRI signals in WM.

Regarding the methodological aspect, although both GM and WM networks were constructed by using the correlations of resting-state fMRI BOLD signals, there were several differences in the data processing procedures for GM and WM. First, the ways to extract the time series data from WM and GM are different from each other. The traditional average calculated across voxels (equal weight) within an ROI was used for GM regions, whereas the TBSS weighted method (unequal weight) was used for WM regions. Second, in our previous study (Jiang et al., 2019b), the middle and deep WM exhibited the maximal amplitude at the frequency of 0.07 Hz and the main frequency component located at the frequency band of 0.01–0.15 Hz. Thus, the filtering band is different when building WM and GM networks. The main findings in the current study were the differences between the SZ and HC groups. It should be further investigated how the differences in the frequency band could have influenced

WM and GM networks. Finally, previous methods had substantial issues due to spatial smoothing, which exacerbated the possible contribution of GM (or other issues) to WM due to partial-volume effects. By projecting the functional BOLD signals onto the structural FA skeleton of WM, this approach may hopefully resolve the issue of spatial smoothing in WM function analysis.

Several limitations should be considered when interpreting our findings. First, most patients had chronic SZ and were taking anti-psychotics. It is difficult to rule out the potential effect of the medication. Second, cognitive measures were not evaluated; thus, we can only speculate possible associations between disruptions in WM network function and cognitive deficits in SZ. Third, as impaired information processing, such as lower intelligence quotient (IQ), which is related to educational level and brain measures, is likely part of the illness, matching on the educational level between patients and healthy controls may lead to an underestimation of effects and loss of some of the relevant information. Thus, matching on parental level of education (Ray et al., 2017) is more appropriate in the future work. In addition, the current study has a cross-sectional design and could not uncover the dynamic changes over time in SZ. In addition, the association between observed BOLD signals in WM and neuron-related activity remains unclear (Gawryluk, Mazerolle, & D'Arcy, 2014b). As WM tracts cross each other, it is extremely difficult to locate the precise source of the functional signals in WM. In node definition, we used a verified WM atlas to segment the WM tract rather than data-driven methods (such as cluster analysis and independent component analysis) or a random segmentation strategy because of its inherent practicality, comparability and anatomical information. Finally, the conclusions of this study are from only one cohort, which needs to be further verified by other samples in future work.

In summary, our findings provide evidence for abnormal global topological properties in SZ, involving reduced local

efficiency, cluster coefficients, hierarchy, small-worldness and increased synchronization, from the perspective of the WM functional network in the brain. Interestingly, patients with SZ showed enhanced centralities in parietal and occipital GM areas; however, adjacent WM tracts (optic radiation, posterior corona radiata and splenium of corpus callosum), which connect those GM regions, exhibited reduced nodal centralities, suggesting that WM functional alterations may play a possible compensatory role for adjacent GM impairments in SZ.

Supplementary material. The supplementary material for this article can be found at <https://doi.org/10.1017/S0033291720003141>.

Data availability. The data supporting the findings of this study are available from the corresponding author upon reasonable request.

Acknowledgements. We are grateful to all the participants in this study. Our thanks also go to Dr Xi Chen (Civil Aviation Flight University of China) for her help to collect the dataset. This work was partly supported by the grant from the National Key R&D Program of China (No. 2018YFA0701400), grants from the National Natural Science Foundation of China (No. grant number: 61933003, 81771822, 81861128001, and 81771925), the CAMS Innovation Fund for Medical Sciences (CIFMS) (No. 2019-12M-5-039) and the Project of Science and Technology Department of Sichuan Province (No. 2019YJ0179).

Author contributions.

Cheng Luo and Dezhong Yao contributed equally to supervise and to design the study; Jingyu Zhou, Huang Huan, Meiling Wang and Mingjun Duan managed the experiments and data collection; Yuchao Jiang, Xin Chang and Yue Tan undertook the data analysis; Yuchao Jiang and Cheng Luo wrote and revised the manuscript. All authors reviewed the manuscript and approved the final manuscript.

Conflict of interest. There is no conflict of interest.

References

- Agcaoglu, O., Miller, R., Damaraju, E., Rashid, B., Bustillo, J., Cetin, M. S., ... Calhoun, V. D. (2018). Decreased hemispheric connectivity and decreased intra- and inter-hemisphere asymmetry of resting state functional network connectivity in schizophrenia. *Brain Imaging and Behavior*, *12*(3), 615–630. doi: 10.1007/s11682-017-9718-7.
- Aydin, K., Uçok, A., & Guler, J. (2008). Altered metabolic integrity of corpus callosum among individuals at ultra high risk of schizophrenia and first-episode patients. *Biological Psychiatry*, *64*(9), 750–757. doi: 10.1016/j.biopsych.2008.04.007.
- Barahona, M., & Pecora, L. M. (2002). Synchronization in small-world systems. *Physical Review Letters*, *89*(5), 054101. doi: 10.1103/PhysRevLett.89.054101.
- Barbatesi, P., Fabri, M., & Mensa, E. (2014). Characterization of NO-producing neurons in the rat corpus callosum. *Brain and Behavior*, *4*(3), 317–336. doi: 10.1002/brb3.218.
- Bassett, D. S., Bullmore, E., Verchinski, B. A., Mattay, V. S., Weinberger, D. R., & Meyer-Lindenberg, A. (2008). Hierarchical organization of human cortical networks in health and schizophrenia. *Journal of Neuroscience*, *28*(37), 9239–9248. doi: 10.1523/JNEUROSCI.1929-08.2008.
- Beaulieu, C. (2002). The basis of anisotropic water diffusion in the nervous system – a technical review. *Nmr in Biomedicine*, *15*(7–8), 435–455. doi: 10.1002/nbm.782.
- Bora, E., Fornito, A., Radua, J., Walterfang, M., Seal, M., Wood, S. J., ... Pantelis, C. (2011). Neuroanatomical abnormalities in schizophrenia: A multimodal voxelwise meta-analysis and meta-regression analysis. *Schizophrenia Research*, *127*(1–3), 46–57. doi: 10.1016/j.schres.2010.12.020.
- Bullmore, E., & Sporns, O. (2009). Complex brain networks: Graph theoretical analysis of structural and functional systems. *Nature Reviews Neuroscience*, *10*(3), 186–198. doi: 10.1038/nrn2575.
- Chen, Z., Hu, X., Chen, Q., & Feng, T. (2019). Altered structural and functional brain network overall organization predict human intertemporal decision-making. *Human Brain Mapping*, *40*(1), 306–328. doi: 10.1002/hbm.24374.
- Chen, X., Liu, C., He, H., Chang, X., Jiang, Y., Li, Y., ... Yao, D. (2017a). Transdiagnostic differences in the resting-state functional connectivity of the prefrontal cortex in depression and schizophrenia. *Journal of Affective Disorders*, *217*, 118–124. doi: 10.1016/j.jad.2017.04.001.
- Chen, X., Zhang, H., Zhang, L., Shen, C., Lee, S. W., & Shen, D. (2017b). Extraction of dynamic functional connectivity from brain grey matter and white matter for MCI classification. *Human Brain Mapping*, *38*(10), 5019–5034. doi: 10.1002/hbm.23711.
- Courtemanche, M. J., Sparrey, C. J., Song, X., MacKay, A., & D’Arcy, R. C. N. (2018). Detecting white matter activity using conventional 3 Tesla fMRI: An evaluation of standard field strength and hemodynamic response function. *Neuroimage*, *169*, 145–150. doi: 10.1016/j.neuroimage.2017.12.008.
- Desikan, R. S., Segonne, F., Fischl, B., Quinn, B. T., Dickerson, B. C., Blacker, D., ... Killiany, R. J. (2006). An automated labeling system for subdividing the human cerebral cortex on MRI scans into gyral based regions of interest. *Neuroimage*, *31*(3), 968–980. doi: 10.1016/j.neuroimage.2006.01.021.
- Dong, D., Luo, C., Guell, X., Wang, Y., He, H., Duan, M., ... Yao, D. (2020). Compression of cerebellar functional gradients in schizophrenia. *Schizophrenia Bulletin*. doi: 10.1093/schbul/sbaa016.
- Dong, D., Wang, Y., Chang, X., Luo, C., & Yao, D. (2018). Dysfunction of large-scale brain networks in schizophrenia: A meta-analysis of resting-state functional connectivity. *Schizophrenia Bulletin*, *44*(1), 168–181. doi: 10.1093/schbul/sbx034.
- Duan, M., Chen, X., He, H., Jiang, Y., Jiang, S., Xie, Q., ... Yao, D. (2015). Altered basal ganglia network integration in schizophrenia. *Frontiers in Human Neuroscience*, *9*, 561. doi: 10.3389/fnhum.2015.00561.
- Fan, Y. S., Li, Z., Duan, X., Xiao, J., Guo, X., Han, S., ... Chen, H. (2020). Impaired interactions among white-matter functional networks in antipsychotic-naïve first-episode schizophrenia. *Human Brain Mapping*, *41*(1), 230–240. doi: 10.1002/hbm.24801.
- Ford, J. M., Krystal, J. H., & Mathalon, D. H. (2007). Neural synchrony in schizophrenia: From networks to new treatments. *Schizophrenia Bulletin*, *33*(4), 848–852. doi: 10.1093/schbul/sbm062.
- Fornito, A., Zalesky, A., Pantelis, C., & Bullmore, E. T. (2012). Schizophrenia, neuroimaging and connectomics. *Neuroimage*, *62*(4), 2296–2314. doi: 10.1016/j.neuroimage.2011.12.090.
- Fries, P. (2009). Neuronal gamma-band synchronization as a fundamental process in cortical computation. *Annual Review of Neuroscience*, *32*, 209–224. doi: 10.1146/annurev.neuro.051508.135603.
- Gawryluk, J. R., Mazerolle, E. L., Beyea, S. D., & D’Arcy, R. C. (2014a). Functional MRI activation in white matter during the Symbol Digit Modalities Test. *Frontiers in Human Neuroscience*, *8*, 589. doi: 10.3389/fnhum.2014.00589.
- Gawryluk, J. R., Mazerolle, E. L., & D’Arcy, R. C. (2014b). Does functional MRI detect activation in white matter? A review of emerging evidence, issues, and future directions. *Frontiers in Neuroscience*, *8*, 239. doi: 10.3389/fnins.2014.00239.
- Gong, J., Luo, C., Li, X., Jiang, S., Khundrakpam, B. S., Duan, M., ... Yao, D. (2019). Evaluation of functional connectivity in subdivisions of the thalamus in schizophrenia. *British Journal of Psychiatry*, *214*(5), 288–296. doi: 10.1192/bjp.2018.299.
- Guo, W., Liu, F., Liu, J., Yu, L., Zhang, J., Zhang, Z., ... Zhao, J. (2015). Abnormal causal connectivity by structural deficits in first-episode, drug-naïve schizophrenia at rest. *Schizophrenia Bulletin*, *41*(1), 57–65. doi: 10.1093/schbul/sbu126.
- Ho, N. F., Iglesias, J. E., Sum, M. Y., Kuswanto, C. N., Sitoh, Y. Y., De Souza, J., ... Holt, D. J. (2017). Progression from selective to general involvement of hippocampal subfields in schizophrenia. *Molecular Psychiatry*, *22*(1), 142–152. doi: 10.1038/mp.2016.4.
- Huang, Y., Bailey, S. K., Wang, P., Cutting, L. E., Gore, J. C., & Ding, Z. (2018). Voxel-wise detection of functional networks in white matter. *Neuroimage*, *183*, 544–552. doi: 10.1016/j.neuroimage.2018.08.049.
- Ji, G. J., Liao, W., Chen, F. F., Zhang, L., & Wang, K. (2017). Low-frequency blood oxygen level-dependent fluctuations in the brain white matter: More than just noise. *Science Bulletin*, *62*(9), 656–657. doi: 10.1016/j.scib.2017.03.021.

- Ji, G. J., Ren, C., Li, Y., Sun, J., Liu, T., Gao, Y., ... Wang, K. (2019). Regional and network properties of white matter function in Parkinson's disease. *Human Brain Mapping, 40*(4), 1253–1263. doi: 10.1002/hbm.24444.
- Jiang, Y., Duan, M., Chen, X., Zhang, X., Gong, J., Dong, D., ... Yao, D. (2019a). Aberrant prefrontal-thalamic-cerebellar circuit in schizophrenia and depression: Evidence from a possible causal connectivity. *International Journal of Neural Systems, 29*(5), 1850032. doi: 10.1142/S0129065718500326.
- Jiang, Y., Luo, C., Li, X., Duan, M., He, H., Chen, X., ... Yao, D. (2018). Progressive reduction in gray matter in patients with schizophrenia assessed with MR imaging by using causal network analysis. *Radiology, 287*(2), 633–642. doi: 10.1148/radiol.2017171832.
- Jiang, Y., Luo, C., Li, X., Li, Y., Yang, H., Li, J., ... Yao, D. (2019b). White-matter functional networks changes in patients with schizophrenia. *Neuroimage, 190*, 172–181. doi: 10.1016/j.neuroimage.2018.04.018.
- Jiang, Y., Song, L., Li, X., Zhang, Y., Chen, Y., Jiang, S., ... Luo, C. (2019c). Dysfunctional white-matter networks in medicated and unmedicated benign epilepsy with centrotemporal spikes. *Human Brain Mapping, 40*(10), 3113–3124. doi: 10.1002/hbm.24584.
- Kochunov, P., & Hong, L. E. (2014). Neurodevelopmental and neurodegenerative models of schizophrenia: White matter at the center stage. *Schizophrenia Bulletin, 40*(4), 721–728. doi: 10.1093/schbul/sbu070.
- Li, J., Biswal, B. B., Wang, P., Duan, X., Cui, Q., Chen, H., & Liao, W. (2019a). Exploring the functional connectome in white matter. *Human Brain Mapping, 40*(15), 4331–4344. doi: 10.1002/hbm.24705.
- Li, M., Newton, A. T., Anderson, A. W., Ding, Z., & Gore, J. C. (2019b). Characterization of the hemodynamic response function in white matter tracts for event-related fMRI. *Nature Communications, 10*(1), 1140. doi: 10.1038/s41467-019-09076-2.
- Liu, Y., Liang, M., Zhou, Y., He, Y., Hao, Y., Song, M., ... Jiang, T. (2008). Disrupted small-world networks in schizophrenia. *Brain, 131*(Pt 4), 945–961. doi: 10.1093/brain/awn018.
- Lo, C. Y., Su, T. W., Huang, C. C., Hung, C. C., Chen, W. L., Lan, T. H., ... Bullmore, E. T. (2015). Randomization and resilience of brain functional networks as systems-level endophenotypes of schizophrenia. *Proceedings of the National Academy of Sciences of the United States of America, 112*(29), 9123–9128. doi: 10.1073/pnas.1502052112.
- Luo, Y., He, H., Duan, M., Huang, H., Hu, Z., Wang, H., ... Luo, C. (2019). Dynamic functional connectivity strength within different frequency-band in schizophrenia. *Frontiers in Psychiatry, 10*, 995. doi: 10.3389/fpsy.2019.00995.
- Lynall, M. E., Bassett, D. S., Kerwin, R., McKenna, P. J., Kitzbichler, M., Muller, U., & Bullmore, E. (2010). Functional connectivity and brain networks in schizophrenia. *Journal of Neuroscience, 30*(28), 9477–9487. doi: 10.1523/JNEUROSCI.0333-10.2010.
- Makedonov, I., Chen, J. J., Masellis, M., & MacIntosh, B. J., & Alzheimer's Disease Neuroimaging, I. (2016). Physiological fluctuations in white matter are increased in Alzheimer's disease and correlate with neuroimaging and cognitive biomarkers. *Neurobiology of Aging, 37*, 12–18. doi: 10.1016/j.neurobiolaging.2015.09.010.
- Marussich, L., Lu, K. H., Wen, H., & Liu, Z. (2017). Mapping white-matter functional organization at rest and during naturalistic visual perception. *Neuroimage, 146*, 1128–1141. doi: 10.1016/j.neuroimage.2016.10.005.
- McCutcheon, R. A., Abi-Dargham, A., & Howes, O. D. (2019). Schizophrenia, dopamine and the striatum: From biology to symptoms. *Trends in Neurosciences, 42*(3), 205–220. doi: 10.1016/j.tins.2018.12.004.
- Menon, V. (2011). Large-scale brain networks and psychopathology: A unifying triple network model. *Trends in Cognitive Sciences, 15*(10), 483–506. doi: 10.1016/j.tics.2011.08.003m
- Moran, L. V., Tagamets, M. A., Sampath, H., O'Donnell, A., Stein, E. A., Kochunov, P., & Hong, L. E. (2013). Disruption of anterior insula modulation of large-scale brain networks in schizophrenia. *Biological Psychiatry, 74*(6), 467–474. doi: 10.1016/j.biopsych.2013.02.029.
- Peer, M., Nitzan, M., Bick, A. S., Levin, N., & Arzyt, S. (2017). Evidence for functional networks within the human brain's white matter. *Journal of Neuroscience, 37*(27), 6394–6407. doi: 10.1523/Jneurosci.3872-16.2017.
- Pergola, G., Selvaggi, P., Trizio, S., Bertolino, A., & Blasi, G. (2015). The role of the thalamus in schizophrenia from a neuroimaging perspective. *Neuroscience and Biobehavioral Reviews, 54*, 57–75. doi: 10.1016/j.neubiorev.2015.01.013.
- Petzold, G. C., & Murthy, V. N. (2011). Role of astrocytes in neurovascular coupling. *Neuron, 71*(5), 782–797. doi: 10.1016/j.neuron.2011.08.009.
- Rash, J. E. (2010). Molecular disruptions of the panglial syncytium block potassium siphoning and axonal saltatory conduction: Pertinence to neuromyelitis optica and other demyelinating diseases of the central nervous system. *Neuroscience, 168*(4), 982–1008. doi: 10.1016/j.neuroscience.2009.10.028.
- Ray, K. L., Lesh, T. A., Howell, A. M., Salo, T. P., Ragland, J. D., MacDonald, A. W., ... Carter, C. S. (2017). Functional network changes and cognitive control in schizophrenia. *NeuroImage-Clinical, 15*, 161–170. doi: 10.1016/j.nicl.2017.05.001.
- Rosenberger, G., Nestor, P. G., Oh, J. S., Levitt, J. J., Kindlerman, G., Bouix, S., ... Kubicki, M. (2012). Anterior limb of the internal capsule in schizophrenia: A diffusion tensor tractography study. *Brain Imaging and Behavior, 6*(3), 417–425. doi: 10.1007/s11682-012-9152-9.
- Rubinov, M., & Sporns, O. (2010). Complex network measures of brain connectivity: Uses and interpretations. *Neuroimage, 52*(3), 1059–1069. doi: 10.1016/j.neuroimage.2009.10.003.
- Sellgren, C. M., Gracias, J., Watmuff, B., Biag, J. D., Thanos, J. M., Whittredge, P. B., ... Perlis, R. H. (2019). Increased synapse elimination by microglia in schizophrenia patient-derived models of synaptic pruning. *Nature Neuroscience, 22*(3), 374. doi: 10.1038/s41593-018-0334-7.
- Shen, K., Mistic, B., Cipollini, B. N., Bezgin, G., Buschkuhl, M., Hutchison, R. M., ... Berman, M. G. (2015). Stable long-range interhemispheric coordination is supported by direct anatomical projections. *Proceedings of the National Academy of Sciences of the United States of America, 112*(20), 6473–6478. doi: 10.1073/pnas.1503436112.
- Smith, A. J., Blumenfeld, H., Behar, K. L., Rothman, D. L., Shulman, R. G., & Hyder, F. (2002). Cerebral energetics and spiking frequency: The neurophysiological basis of fMRI. *Proceedings of the National Academy of Sciences of the United States of America, 99*(16), 10765–10770. doi: 10.1073/pnas.132272199.
- Uhlhaas, P. J., Haenschel, C., Nikolic, D., & Singer, W. (2008). The role of oscillations and synchrony in cortical networks and their putative relevance for the pathophysiology of schizophrenia. *Schizophrenia Bulletin, 34*(5), 927–943. doi: 10.1093/schbul/sbn062.
- Uhlhaas, P. J., & Singer, W. (2010). Abnormal neural oscillations and synchrony in schizophrenia. *Nature Reviews Neuroscience, 11*(2), 100–113. doi: 10.1038/nrn2774.
- Wang, J., Jiang, Y., Tang, Y., Xia, M., Curtin, A., Li, J., ... Wang, J. (2020). Altered functional connectivity of the thalamus induced by modified electroconvulsive therapy for schizophrenia. *Schizophrenia Research, 2020*. doi: 10.1016/j.schres.2019.12.044.
- Wang, Q., Zhang, J., Liu, Z., Crow, T. J., Zhang, K., Palaniyappan, L., ... Li, T. (2019). "Brain connectivity deviates by Sex and hemisphere in the first episode of schizophrenia" – a route to the genetic basis of language and psychosis? *Schizophrenia Bulletin, 45*(2), 484–494. doi: 10.1093/schbul/sby061.
- Whitford, T. J., Kubicki, M., Schneiderman, J. S., O'Donnell, L. J., King, R., Alvarado, J. L., ... Shenton, M. E. (2010). Corpus callosum abnormalities and their association with psychotic symptoms in patients with schizophrenia. *Biological Psychiatry, 68*(1), 70–77. doi: 10.1016/j.biopsych.2010.03.025.
- Wu, T. L., Wang, F., Li, M., Schilling, K. G., Gao, Y., Anderson, A. W., ... Gore, J. C. (2019). Resting-state white matter-cortical connectivity in non-human primate brain. *Neuroimage, 184*, 45–55. doi: 10.1016/j.neuroimage.2018.09.021.
- Wu, X., Yang, Z., Bailey, S. K., Zhou, J., Cutting, L. E., Gore, J. C., & Ding, Z. (2017). Functional connectivity and activity of white matter in somatosensory pathways under tactile stimulations. *Neuroimage, 152*, 371–380. doi: 10.1016/j.neuroimage.2017.02.074.
- Yang, C., Zhang, W., Yao, L., Liu, N., Shah, C., Zeng, J., ... Lui, S. (2019). Functional alterations of white matter in chronic never-treated and treated schizophrenia patients. *Journal of Magnetic Resonance Imaging, 2019*. doi: 10.1002/jmri.27028.
- Yu, M., Dai, Z., Tang, X., Wang, X., Zhang, X., Sha, W., ... Zhang, Z. (2017). Convergence and divergence of brain network dysfunction in deficit and non-deficit schizophrenia. *Schizophrenia Bulletin, 43*(6), 1315–1328. doi: 10.1093/schbul/sbx014.